stone replacement and nucleosome loss associated with transcription in vivo (*9*, *40*, *41*). The further development of assays to capture the movements of physiologically marked histones should provide insight into the regulation of chromatin dynamics.

Note added in proof: The subunits of the SWR1 complex—Vps72, Swc1, God1, Aor1, and Vps71—have been renamed Swc2, Swc3, Swc4, Swc5, and Swc6, respectively, by agreement with the laboratories of J. Greenblatt, H. Madhani, and J. Rine.

References and Notes

1. R. D. Kornberg, Y. Lorch, *Cell* **98**, 285 (1999).
2. G. J. Narlikar, H. Y. Fan, R. E. Kingston, *Cell* **108**, 475 (2002).
3. W. Fischle, Y. Wang, C. D. Allis, *Curr. Opin. Cell Biol.* **15**, 172 (2003).
4. J. A. Martens, F. Winston, *Curr. Opin. Genet. Dev.* **13**, 136 (2003).
5. P. B. Becker, W. Horz, *Annu. Rev. Biochem.* **71**, 247 (2002).
6. K. E. Van Holde, *Chromatin* (Springer-Verlag, New York, 1989).
7. C. Redon *et al.*, *Curr. Opin. Genet. Dev.* **12**, 162 (2002).
8. M. M. Smith, *Curr. Opin. Cell Biol.* **14**, 279 (2002).
9. K. Ahmad, S. Henikoff, *Proc. Natl. Acad. Sci. U.S.A.* **99** (suppl. 4), 16477 (2002).
10. M. J. Clarkson, J. R. E. Wells, F. Gibson, R. Saint, D. J. Tremethick, *Nature* **399**, 694 (1999).
11. C. L. Hatch, W. M. Bonner, E. N. Moudrianakis, *Science* **221**, 468 (1983).
12. R. K. Suto, M. J. Clarkson, D. J. Tremethick, K. Luger, *Nat. Struct. Biol.* **7**, 1121 (2000).
13. M. D. Meneghini, M. Wu, H. D. Madhani, *Cell* **112**, 725 (2003).
14. I. A. Olave, S. L. Reck-Peterson, G. R. Crabtree, *Annu. Rev. Biochem.* **71**, 755 (2002).
15. X. Shen, G. Mizuguchi, A. Hamiche, C. Wu, *Nature* **406**, 541 (2000).
16. X. Shen, R. Ranallo, E. Choi, C. Wu, *Mol. Cell* **12**, 147 (2003).
17. More information is available online at www.yeastgenome.org.
18. Materials and methods are available as supporting material on *Science* Online.
19. G. Mizuguchi *et al.*, unpublished observations.
20. H. V. Goodson, W. F. Hawse, *J. Cell Sci.* **115**, 2619 (2002).
21. P. M. Ayton, M. L. Cleary, *Oncogene* **20**, 5695 (2001).
22. Y. Ishimi, A. Kikuchi, *J. Biol. Chem.* **266**, 7025 (1991).
23. M. Hampsey, *Yeast* **13**, 1099 (1997).
24. T. J. Begley, A. S. Rosenbach, T. Ideker, L. D. Samson, *Mol. Cancer Res.* **1**, 103 (2002).
25. M. E. Gelbart, T. Rechsteiner, T. J. Richmond, T. Tsukiyama, *Mol. Cell. Biol.* **21**, 2098 (2001).
26. K. Luger, T. J. Rechsteiner, T. J. Richmond, *Methods Enzymol.* **304**, 3 (1999).
27. T. Fazzio, T. Tsukiyama, *Mol. Cell* **12**, 1333 (2003).
28. S. R. Kassabov, B. Zhang, J. Persinger, B. Bartholomew, *Mol. Cell* **11**, 391 (2003).
29. A. Saha, J. Wittmeyer, B. R. Cairns, *Genes Dev.* **16**, 2120 (2002).
30. I. Whitehouse, C. Stockdale, A. Flaus, M. D. Szczelkun, T. Owen-Hughes, *Mol. Cell. Biol.* **23**, 1935 (2003).
31. K. E. Van Holde, J. Zlatanova, G. Arents, E. Moudrianakis, *Chromatin Structure and Gene Expression* (Oxford Univ. Press, ed. 1, 1995).
32. T. J. Richmond, J. Widom, *Chromatin Structure and Gene Expression* (Oxford Univ. Press. ed. 2, 2000).
33. Y. Nakatani, J. Rine, J. Greenblatt, personal communication.
34. As an example, stoichiometric binding of FACT (facilitates chromatin transcription) assists displacement of H2A-H2B dimers (*42*).
35. M. Harata *et al.*, *Mol. Biol. Cell* **10**, 2595 (1999).
36. L. Galarneau *et al.*, *Mol. Cell* **5**, 927 (2000).
37. H. Szerlong, A. Saha, B. R. Cairns, *EMBO J.* **22**, 3175 (2003).
38. M. M. Smith, personal communication.
39. The RSC complex is required (apparently indirectly) for deposition of the centromere-specific histone variant Cse4 (*43*).
40. H. Boeger, J. Griesenbeck, J. S. Strattan, R. D. Kornberg, *Mol. Cell* **11**, 1587 (2003).
41. H. Reinke, W. Horz, *Mol. Cell* **11**, 1599 (2003).
42. M. Belotserkovskaya *et al.*, *Science* **301**, 1090 (2003).
43. J. M. Hsu, J. Huang, P. B. Meluh, B. C. Laurent, *Mol. Cell Biol.* **23**, 3202 (2003).
44. Data is available at http://home.ccr.cancer.gov/landrydata803/.

45. We thank Y. Natakani and H. Tagami for stimulating discussions; T. Tsukiyama, K. Luger, M. Lichten, and members of their laboratories for reagents, histone protocols, and advice; J. Delrow for advice on microarray analysis; W. Lane for protein microsequencing; T. Tsukiyama, J. Palmer, and R. Ranallo for initial studies; J. Widom for a nucleosome positioning sequence; and Y. Nakatani, J. Rine, M. Smith, T. Tsukiyama, J. Greenblatt, J. Cote, and P. Silver for communicating unpublished results. This work was supported by the National Cancer Institute.

Supporting Online Material

www.sciencemag.org/cgi/content/full/1090701/DC1
Materials and Methods
Figs. S1 to S5
Tables S1 to S3
References

22 August 2003; accepted 11 November 2003
Published online 27 November 2003;
10.1126/science.1090701
Include this information when citing this paper.

REPORTS

Self-Assembly of Mesoscopic Metal-Polymer Amphiphiles

Sungho Park, Jung-Hyurk Lim, Sung-Wook Chung, Chad A. Mirkin*

The assembly properties of two- and three-component rod-like building blocks consisting of gold and polymer block domains have been investigated. These structures behave like mesoscopic amphiphiles and form a series of single-layer superstructures consisting of bundles, tubes, and sheets depending upon the compositional periodicity. Unlike molecular systems, the template used to initially synthesize them plays a critical role in the assembly process by pre-aligning them in a manner that facilitates their assembly by optimizing the correct collisional orientation upon dissolution of the template. Tubular structures with tailorable diameters can be assembled in a predictable manner on the basis of an estimate of the hybrid rod packing parameters.

Over the past decade, major advances have been made in the synthesis and characterization of one-dimensional rod-like nanostructures (*1*). One can now synthesize, via a variety of routes, carbon-based nanotubes, polymer structures, and metal, semiconducting, and insulator inorganic compositions (*2*–*8*). These materials have several unusual and potentially useful properties that make them promising for many potential applications in optics (*9*), electronics (*10*), and biodiagnostics (*6*). One of the most powerful and now extensively used methods for synthesizing such structures relies on solid-state templates and electrochemistry to control the diameter and length of such structures (*6*, *11*). Using this approach, one can synthesize one- and multicomponent structures with exquisite control over block composition size. Although these rod-like building blocks can be routinely made in large quantities and in massively parallel fashion, only a few techniques allow one to assemble them into organized two- and three-dimensional structures (*12*–*17*). No techniques have been developed for controlling their assembly into curved structures, a capability necessary to fully understand and exploit the concept of self-assembly with unnatural mesoscopic building blocks (*18*).

Our approach to generating mesoscopic amphiphiles involves the synthesis of rod-like structures consisting of hard and soft domains. The hard hydrophilic domain is an inorganic material such as gold, and the soft domain is a hydrophobic conducting polymer such as oxidized polypyrrole, which can be electrochemically polymerized within the confines of an alumina template. The rationale was that because of the compositional differences between the inorganic and organic portions of these novel structures, the

Department of Chemistry and Institute for Nanotechnology, Northwestern University, 2145 Sheridan Road, Evanston, IL 60208–3113, USA.

*To whom correspondence should be addressed. E-mail: camirkin@chem.northwestern.edu

block ends would tend to phase segregate in a way that would align the structures to maximize interactions between blocks of similar composition, akin to block copolymers (*19*) but different with respect to size and the fact that one block is made of a rigid inorganic material. To test this hypothesis, we synthesized a series of rod structures that varied in polymer and gold block lengths.

In a typical experiment, segmented metal-polymer rods were prepared by electrodeposition of gold into porous aluminum templates (*20*) via the method of Martin and co-workers (*11*), followed by electrochemical polymerization of pyrrole. The length of each block can be controlled by monitoring the charge passed during the electrodeposition process (*20*). After the rods have been formed, they are released from the template by dissolving it with 3 M NaOH. The rods are centrifuged (5000 revolutions per minute for 10 min), rinsed several times with NANOpure (Barnstead International, Dubuque, IA) water, and then resuspended in water by vortexing for 1 min. Four different rod structures were studied as a function of block composition and ratio. One three-component structure consisting of Au ends with a polymer interior was investigated as well (Table 1).

When the rods are released from the template and imaged by scanning electron microscopy (SEM), one can see that the polymer portions of the rods have a diameter that is smaller than the gold portions (Fig. 1A, inset, lower right). This has been confirmed by atomic force microscopy as well (*20*). For all rods generated for these studies, the average Au block diameter was 400 (±30) nm, and the polypyrrole block diameter was 360 (±25) nm. These structures self-organize into mesoscopic architectures with unusual structures, including bundles, tubes of varying diameters, and sheets. For example, amphiphilic rods with an Au block length of 1.8 (±0.2) μm and a polymer block length of 8.8 (±1.3) μm form bundle structures (Fig. 1A). These structures have been characterized by SEM (Fig. 1A) and optical microscopy (*20*). About 70% of the rods make up the bundle structures, with the other 30% being freely dispersed in solution.

It has been reported that miniaturized triblock copolymers containing rigid biphenyl ester blocks self-assemble into "mushroom-shaped" supramolecular nanostructures because of their tendency to aggregate through π-π interactions (*21*). There is a strong analogy between such molecule-based organic systems and the mesoscopic metal-polymer rod structures described herein. The driving force for bundle assembly in the rod system is likely the strong interactions between the organic polymer ends of the different rods (Fig. 2B). Note that the polymer ends of these structures are tightly bundled, which results in stress and limits how large the bundle structures can grow before they begin to form tubular structures. These bundle structures are somewhat reminiscent of the recently reported structures formed from magnetic inorganic materials (*22*). However, the nature of the assembly process and the prospect for architectural control substantially differ (see below).

Three-dimensional microscopic tubular architectures composed of gold-polymer rods can be synthesized by adjusting the block lengths of the gold and polymer portions of the hybrid rod structure. Three different gold/polymer ratios were studied with a fixed rod length of 4.5 (±0.5) μm. Rods with a 1:4 gold/polymer ratio formed ~60-μm-diameter tubes where the entire structure consists of a single layer of rods (Fig. 1B). High-magnification SEM images show that the rods that compose these tubular structures are highly ordered, with the gold ends on the

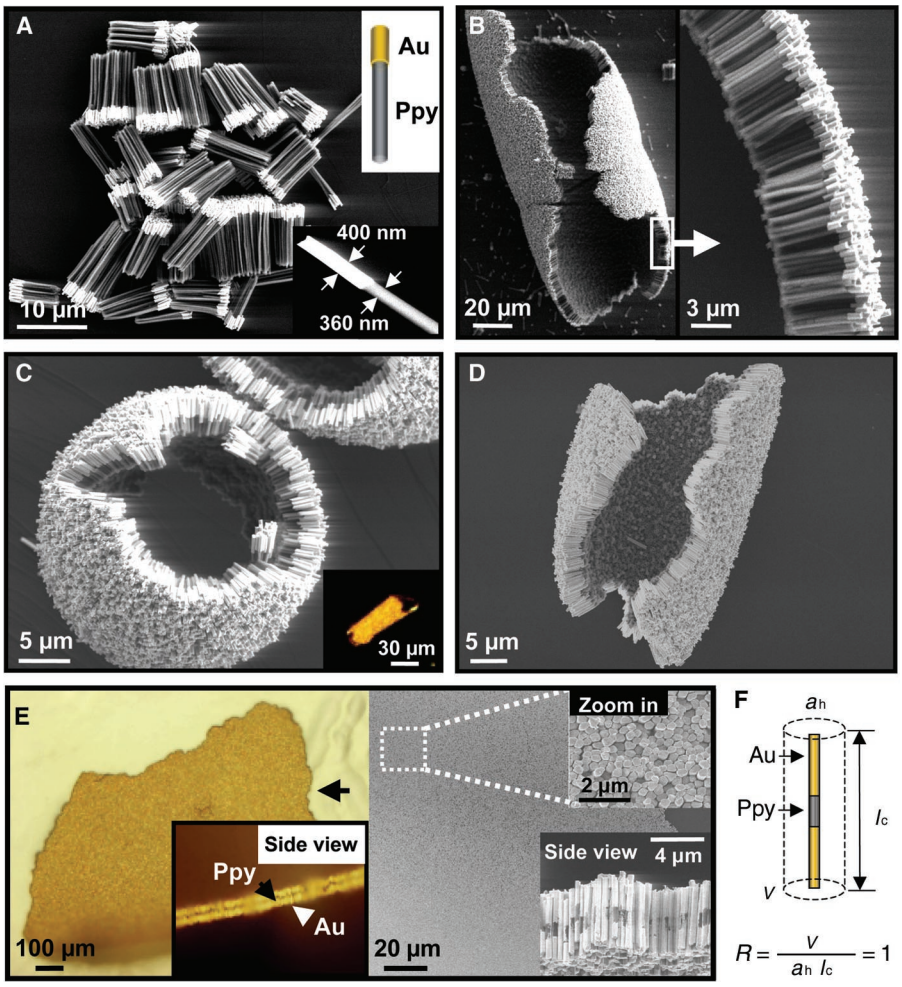

Fig. 1. (**A**) SEM images of Au-Ppy rods. The bright segments are gold, and the dark domains are polypyrrole, corresponding to the diagram in the upper right inset. (Lower right inset) A zoom-in image of a single rod, showing the difference in diameter for the two different blocks. (**B**) SEM images of assemblies of Au-Ppy rods with a 1:4 block-length ratio (left), and a zoom-in image, revealing the highly oriented amphiphilic rods (right). (**C**) A SEM image of aggregates formed from Au-Ppy rods with a 3:2 block length ratio. (Inset) An optical microscopy image of a three-dimensional tubular superstructure formed from these rods. (**D**) A SEM image of a tubular assembly of Au-Ppy rods with a 4:1 block length ratio. (**E**) (Left) Optical images of a planar assembly of three-component rods (Au-Ppy-Au). (Inset) A side view of the planar assembly. The bright segments are Au, and the dark domains are Ppy. (Right) SEM images of the planar aggregates. (Inset) A zoom-in image of the planar assembly (top-down), showing their close packing. A side view shows the highly oriented Au and Ppy domains represented by bright and dark segments, respectively. (**F**) A schematic representation of the Au-Ppy-Au three-component rods.

Table 1. Rod building-block lengths and their respective gold/polypyrrole block ratios.

Length of rod (μm)	10.6 ± 1.4	4.5 ± 0.5			
Block composition Block ratio	Au:Ppy 1:4	Au:Ppy 1:4	Au:Ppy 3:2	Au:Ppy 4:1	Au:Ppy:Au 2:1:2

exterior of the structure and the polymer ends all pointing toward the interior of the tubes (Fig. 1B). Rods with a 3:2 gold/polymer ratio also yield tubular structures but with ~29-μm diameters (Fig. 1C). In this case, the process continues until the sheet-like structure of rods completely wraps around on itself to form a closed tube with open ends (Fig. 1C, inset). At present, we are not sure why the ends do not close. This could be due to an insufficient rod feedstock or stress imposed on the system as the ends begin to close.

If rods with a 4:1 gold-to-polymer ratio are used, ~26-μm-diameter open tubular structures are obtained (Fig. 1D). As with the other examples, the entire structure is made of a single layer of rods, and the structures can be made reproducibly. However, in all cases it is difficult to control the termination of the assembly process and the full formation of the tubular structures. The yield of completely closed-wall structures is low (~10%). Many of them exhibit the open-walled architecture illustrated in Fig. 1D. The assembly process involving these mesoscopic rods can be understood, in part, on the basis of theoretical models (*23*) used for cylindrical micelles made of amphiphilic molecules. The geometric packing parameter, $R = V/a_h l_c$, which is commonly adopted in the molecular-level description for micelles or lipid bilayers (*23*), where v is the volume of an individual rod, a_h is the average rod head area, and l_c is the rod length, can be used to predict the types of structures that form on the basis of the ratio of the gold and polymer blocks that make up these rods. Each rod can be modeled as a truncated cone because of the strong interaction between polymer ends and the contraction in diameter of the polymer block on removal from the template (Fig. 2A). The estimated a_h can be acquired from a first-order approximation of the average area occupied by the gold end of each rod in the microtubular structure, which is defined by the perimeter area of the tube divided by the total number of rods that make up the superstructure (Fig. 2, A and B). The head area in this mesoscopic rod system, as in the case of molecule-based micelle formation (*23*), is affected by the attractive interactions between the polymer blocks units and the steric repulsion between the larger-volume adjacent gold domains (Fig. 2B). For a fixed rod length, an increase in polymer block length results in a decrease in a_h, leading to an increase in the packing parameter R. The larger the R value, the less curvature one would expect from the resulting superstructures (Figs. 1, B to D, and 2D). This general trend is what is observed for the three tubular structures reported herein.

One is not limited to tubular assemblies with these novel mesoscopic amphiphiles. By synthesizing rods with polymer domains sandwiched between two gold segments (i.e., gold-polymer-gold, in Fig. 1F), we were able to generate planar "sheet-like" assemblies. Because from a geometrical packing standpoint the rods in this system no longer behave like truncated cones but rather cylindrical structures, their R collapses to unity, resulting in sheet-like structures (Fig. 1, E and F). High-resolution SEM images show that these sheets, like the tubes, consist of a single layer of rods arranged in such a manner that maximizes the larger diameter gold domain–gold domain contacts. The polymer portions also may be interacting at the gold-polymer interface, but this is inconclusive on the basis of the data in hand. Others also have observed two-dimensional assembly of pure hollow polymer nanotubes, formed in an alumina template, after complete removal of the template (*24*).

It is remarkable that the curved tubular and bundle structures form despite the extraordinarily large number of possibilities for rod assembly and the proper configurations required to effect the formation of the single-layer structures with all rods arranged in a head-to-tail fashion. There is a similarity between this observation and Levinthal's paradox for protein folding, which states that most naturally occurring proteins fold reliably and quickly to their native state despite the astronomical number of possible configurations (*25*). Given the size of these structures and their tendency to sediment, there must be an additional influence. Indeed, the alumina template seems to play a critical role in the assembly process by aligning all the rods in close proximity, which maximizes the correct orientational collision frequency. Consistent with this conclusion, we have observed that the self-organization

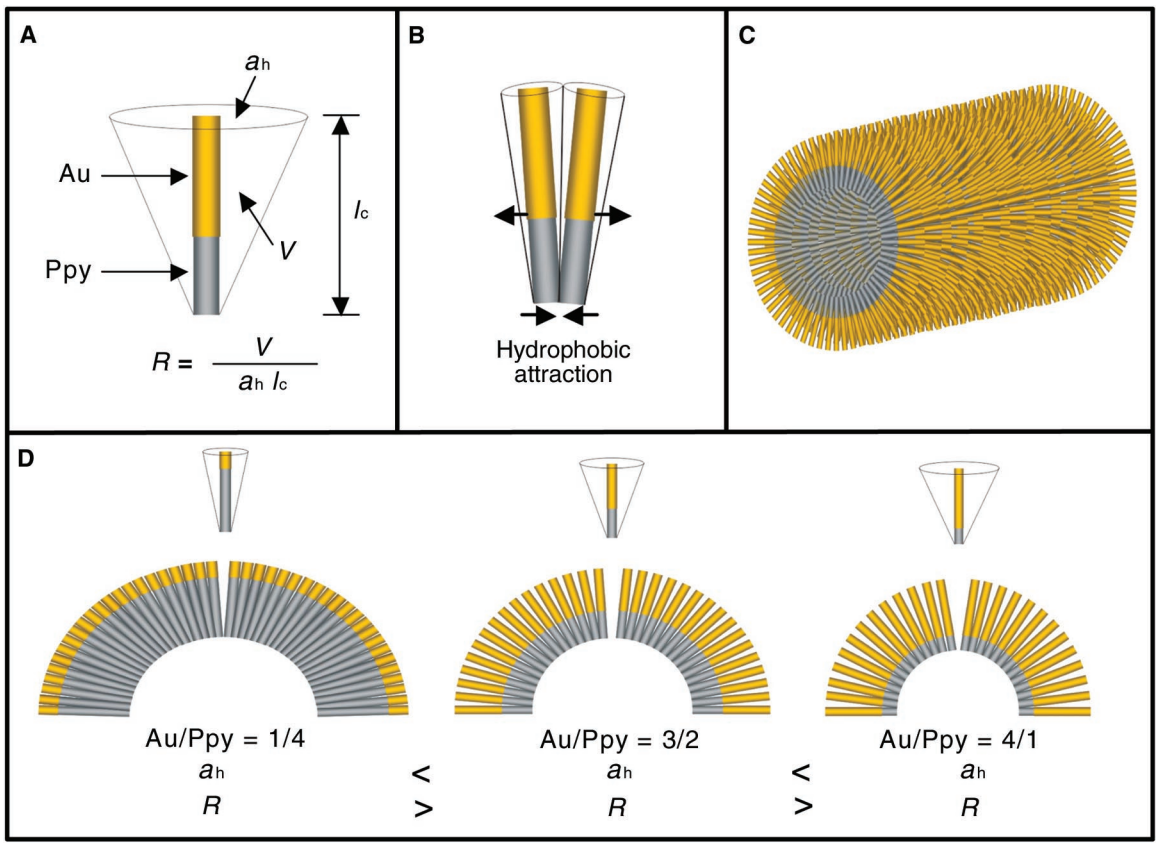

Fig. 2. Schematic representations of the corresponding Au-Ppy rod assemblies described in Fig. 1, B to D. (**A**) Geometric packing parameters (where V is the volume of rods, a_h is the average rod head area, and l_c is the rod length), calculated by assuming a truncated cone. (**B**) The estimated a_h can be acquired from a first-order approximation of the average area occupied by the gold end of each rod in the microtubular structure, which is defined by the perimeter area of the tube divided by the total number of rods that make up the superstructure. (**C**) A three-dimensional tubular structure composed of rod-like building blocks. (**D**) Cross-sectional views of tubes of various diameters formed from specific rod compositions with well-defined block-length ratios.

process is irreversible. Sonication of any of the bundle, tubular, and even sheet-like assemblies results in irreversible dispersion of the rods under all conditions studied thus far, including elevated temperature (80°C, followed by slow cooling). The rate of sedimentation under these conditions effectively competes with the assembly process.

This study has introduced the concept of using polymer segments in nanorod structures to control their assembly into flat two-dimensional and curved three-dimensional structures. One can systematically make different architectures by controlling the composition of the rod structures and the ratio of the blocks of different materials that compose them. Insight into such assembly processes not only complements the work of others with mesoscopic and macroscopic assembly schemes (*26*, *27*) but also is critical to understanding self-organization processes in unnatural systems and the exploitation of these versatile rod-like synthons in the fabrication of a new category of metal-polymer hybrid materials and, perhaps, devices.

References and Notes

1. Y. Xia *et al*., *Adv. Mater.* **15**, 353 (2003).
2. S. Iijima, *Nature* **354**, 56 (1991).
3. H. Dai *et al*., *Chem. Phys. Lett.* **260**, 471 (1996).
4. J. Kong, H. T. Soh, A. M. Cassell, C. F. Quate, H. Dai, *Nature* **395**, 878 (1998).
5. C. R. Martin, *Acc. Chem. Res.* **28**, 61 (1995).
6. S. R. Nicewarner-Pena *et al*., *Science* **294**, 137 (2001).
7. X. Peng *et al*., *Nature* **404**, 59 (2000).
8. G. R. Patzke, F. Krumeich, R. Nesper, *Angew. Chem. Int. Ed. Engl.* **41**, 2446 (2002).
9. X. Duan, Y. Huang, R. Agarwal, C. M. Lieber, *Nature* **421**, 241 (2003).
10. T. Rueckes *et al*., *Science* **289**, 94 (2000).
11. C. R. Martin, *Science* **266**, 1961 (1994).
12. B. Nikoobakht, Z. L. Wang, M. A. El-Sayed, *J. Phys. Chem. B* **104**, 8635 (2000).
13. F. Kim, S. Kwan, J. Akana, P. Yang, *J. Am. Chem. Soc.* **123**, 4360 (2001).
14. E. Dujardin, L.-B. Hsin, C. R. C. Wang, S. Mann, *Chem. Commun.* **2001**, 1264 (2001).
15. N. I. Kovtyukhova, T. E. Mallouk, *Chem. Eur. J.* **8**, 4354 (2002).
16. N. R. Jana *et al*., *J. Mater. Chem.* **12**, 2909 (2002).
17. K. K. Caswell, J. N. Wilson, U. H. F. Bunz, C. J. Murphy, *J. Am. Chem. Soc.* **125**, 13914 (2003).
18. G. A. Ozin, *Can. J. Chem.* **77**, 2001 (1999).
19. N. Hadjichristidis, S. Pispas, G. Floudas, *Block Copolymers: Synthetic Strategies, Physical Properties, and Applications* (Wiley-Interscience, Hoboken, NJ, 2002).
20. Materials and methods are available as supporting material on *Science* Online.
21. S. I. Stupp *et al*., *Science* **276**, 384 (1997).
22. J. C. Love, A. R. Urbach, M. G. Prentiss, G. M. Whitesides, *J. Am. Chem. Soc.* **125**, 12696 (2003).
23. J. N. Israelachvili, *Intermolecular and Surface Forces* (Academic Press, San Diego, CA, 1992).
24. M. Steinhart *et al*., *Science* **296**, 1997 (2002).
25. C. Levinthal, *J. Chim. Phys.* **65**, 44 (1968).
26. A. Terfort, N. Bowden, G. M. Whitesides, *Nature* **386**, 162 (1997).
27. M. J. MacLachlan, N. Coombs, G. A. Ozin, *Nature* **397**, 681 (1999).

28. C.A.M. acknowledges the U.S. Air Force Office of Scientific Research and NSF for supporting this research and G. Schatz for helpful discussions.

Supporting Online Material

www.sciencemag.org/cgi/content/full/303/5656/348/DC1
Materials and Methods
Figs. S1 to S3

4 November 2003; accepted 9 December 2003

Inferences on Flow at the Base of Earth's Mantle Based on Seismic Anisotropy

Mark Panning* and Barbara Romanowicz

We applied global waveform tomography to model radial anisotropy in the whole mantle. We found that in the last few hundred kilometers near the core-mantle boundary, horizontally polarized *S*-wave velocities (V_{SH}) are, on average, faster (by ~1%) than vertically polarized *S*-wave velocities (V_{SV}), suggesting a large-scale predominance of horizontal shear. This confirms that the *D*′′ region at the base of the mantle is also a mechanical boundary layer for mantle convection. A notable exception to this average signature can be found at the base of the two broad low-velocity regions under the Pacific Ocean and under Africa, often referred to as "superplumes," where the anisotropic pattern indicates the onset of vertical flow.

The core-mantle boundary (CMB) represents a thermal and a chemical boundary between Earth's solid silicate mantle and its liquid iron outer core. The corresponding boundary layer on the mantle side, often referred to as *D*′′, is thus the site of complex dynamic processes that may involve thermal and chemical heterogeneity at various scales [e.g., (*1*)]. Additionally, it has been suggested that this layer functions as a mechanical boundary layer for the convection of the overlying mantle, leading to intense deformation. Such deformation processes can lead to detectable seismic anisotropy, either through the alignment of anisotropic crystals in the strain field or through the fine layering of materials with contrasting elastic properties (*2*, *3*).

The presence of anisotropy in *D*′′ has been established in several regions, including under the central Pacific Ocean, northeastern Asia, Alaska, and Central America, from the observation of seismic waves diffracting (S_{diff}) or reflecting (*ScS*) at the CMB (*3*–*8*). The limited areas of sampling, however, have made interpretation of these observations difficult. A more global picture of long-wavelength anisotropic *D*′′ structure would clearly aid interpretation in terms of dynamic flow modeling as well as mineral physics.

With this in mind, we have adapted a global waveform tomography approach (*9*, *10*) to develop a three-dimensional model of radial anisotropy in the whole mantle, using a large data set of three-component time-domain waveforms of surface and body waves (*11*). The model is parameterized in terms of isotropic V_S and the anisotropic ξ parameter ($\xi = V^2_{SH}/V^2_{SV}$), which is directly related to radial anisotropy in *S*-wave velocity (*12*). With our data set and our broadband sensitivity kernels (*9*), which allow us to use both reflected and diffracted waves in *D*′′ (fig. S1), we have enough coverage to invert for radially anisotropic structure in the whole mantle, as shown by resolution tests (*13*).

Our final model includes anisotropic *S*-wave velocity structure throughout the mantle. Two regions of strong "degree 0" radial anisotropy stand out in our model: the uppermost mantle and *D*′′ (Fig. 1). In both regions, on average, V_{SH} is faster than V_{SV}. This can be interpreted, at least for the

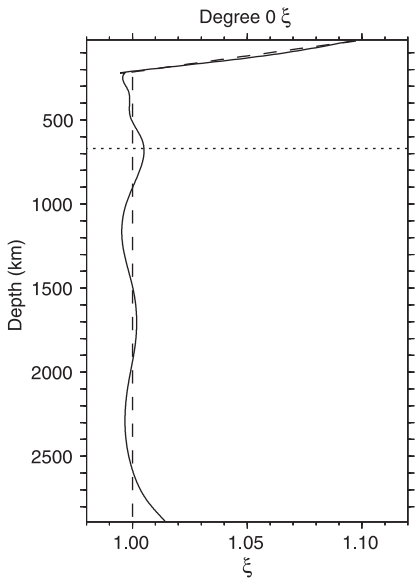

Fig. 1. Degree 0 model for ξ as a function of depth (solid line). The values for PREM (*17*) are shown by the dashed line. For reference, the 660-km discontinuity in the transition zone between the upper and lower mantle is shown (dotted line). Note the strong increase at the base of the mantle, similar but smaller in amplitude to that seen in the uppermost mantle.

Berkeley Seismological Laboratory, 215 McCone Hall, University of California, Berkeley, CA 94720, USA.

*To whom correspondence should be addressed. E-mail: mpanning@seismo.berkeley.edu